International Journal of Pressure Vessels and Piping 202 (2023) 104891

Contents lists available at ScienceDirect

International Journal of Pressure Vessels and Piping

journal homepage: www.elsevier.com/locate/ijpvp

Failure analysis of biocomposite sandwich pipe under internal pressure – Application for high pressure gas transportation pipelines MEDGAZ

Ghania Habbar [a,*], Abdelkader Hocine [a], Abdelhakim Maizia [a], Abderrezak Bezazi [b], João Ribeiro [c,d], Mohamed Houcine Dhaou [e,f], Omar Bouledroua [g]

[a] Controls Laboratory Tests, Measurements and Simulations Mechanics, Hassiba Benbouali University of Chlef, PO. Box 151, Hay Salem, Chlef, Algeria
[b] Laboratory of Applied Mechanics of New Materials LMANM, University 08 May 1945, Guelma, Algeria
[c] Higher School of Technology and Management, Polytechnic Institute of Bragança, 5300-252, Bragança, Portugal
[d] Mountain Research Center, Instituto Politécnico de Bragança, 5300-252, Bragança, Portugal
[e] Department of Physics, College of Science, Qassim University, Buraydah, Almolaydah, 51452, Saudi Arabia
[f] Laboratory of Thermal and Energetic Systems Studies, ENIM, University of Monastir, Ibn Eljazzar Street, Monastir, 5019, Tunisia
[g] SONATRACH/ Central Direction of Research & Development, Avenue November1st, 35000, Boumerdes, Algeria

ARTICLE INFO

Keywords:
Sandwich pipes
biocomposite
Internal pressure
Analytical methods
FEM

ABSTRACT

In this paper, analytical and 3D numerical models are developed to investigate the mechanical behavior of sandwich pipe under internal pressure loading. The suggested models provide an exact solution for stresses, strains and displacement on the sandwich pipe, which is made of epoxy material for the core layer and reinforced materials with an alternate-ply for the skin layers. The aim of this analysis is to evaluate the potential applications of jute and pineapple leaf fiber (PALF) bio-fibers in order to replace glass synthetic fibers generally employed in sandwich pipes. In this subject, a failure analytical analysis was developed using TSAI-WU criterion. The results of stress, strain and displacement distribution through the thickness are presented for the analytical and numerical models. The comparison between the both models results show a very good agreement. In order to increase the rigidity of a biocomposite sandwich and reduce the gap compared with a synthetic sandwich, a gradual reinforcing of layer numbers was chosen, which permitted the best behavior. The ultimate pressure and safety factors obtained by increasing biocomposite layers are significant for composite transportation pressure pipelines, especially for sandwich pipe based on PALF/epoxy.

1. Introduction

The world's interest in gas and oil is climbing steadily, which are definitely the most essential sources of energy on our planet [1]. In the natural gas transportation industry, there will definitely be a rising demand for research, development, and innovation activities. Using composite structures for natural gas transportation systems such as flowlines, gathering pipelines, and distribution pipelines continue to grow [2]. In comparison to many industries, such as building construction, automobiles, and aircraft, where composite materials have been widely used for decades [3], the gas industry has been slow to adopt composites, despite all of composites' benefits and their high potential for use in pipe systems [4]. These structures are becoming more prevalent in the gas industry. Gas transportation infrastructure exists between North Africa and Europe, carrying gas from Algeria and Libya to Europe through Italy and Spain. The volume of gas transported is around 63.5 bcm annually.

Pipelines are essential for natural gas and hydrogen transportation across national and international borders. The steel pipes are installed in various environments and have suffered various damage problems [5]. The most prevalent steel pipe defects are: corrosion damage [[6–19]], cracks [6–8,13,17,20–22], durability [8,13,23,24], maintenance costs [8,14,15,25], buckling and burst piping problems [26].

The usage of composite structures, including pipelines unidirectional multilayer, now represents one of the greatest solutions in the industry, especially for the transport and storage of fluids such as gas, water, and oil [2,27]. Composite pipes are widely recognized and applied in the oil and gas industry due to their benefits of corrosion resistance and structural flexibility can be custom designed, high durability, no need for coating, easy and fast installation, and low maintenance costs [26,

* Corresponding author.
E-mail address: g.habbar93@univ-chlef.dz (G. Habbar).

https://doi.org/10.1016/j.ijpvp.2023.104891
Received 31 October 2022; Received in revised form 30 December 2022; Accepted 9 January 2023
Available online 21 January 2023

28–30]. Not all pipes are manufactured identically. Therefore, the material choice for usage in pipeline systems and hydrocarbon transportation may impact operational costs, maintenance charges, lead time, total cost of ownership, compliance, ease of installation, and many more. There are several composite pipe configurations, including multi-layered cylindrical pipes and sandwich pipes, which are applied in tubular structures.

Multi-layered composite tubes are used in gas and hydrogen transportation due to their high specific strength and stiffness. That's why scientists have performed different research on thick or thin multi-layered composite cylinders [31–36].

While, glass fiber and steel pipes have been widely used for the transportation of oil and gas products also natural gas, sandwich pipes have been explored as one solution to the high-pressure challenges associated with natural gas and hydrogen transport [37,38].

Sandwich pipes are light, versatile composite structures that are composed of three components: the core, internal pipe, and inner pipe [37–41] The last two are dubbed skin.

Sandwich tubes can be circular [1,39,42–45], square [46,47], rectangular [48], or hexagonal [49] in shape.

Synthetic fibers are increasingly being replaced by natural fibers, particularly autochthonous materials [50]. Sadeghian et al. [51] have tested the flexural behavior of a sandwich composite made of flax fiber composite with a cork core and glass fiber composite with a polypropylene core. They discovered that sandwich composites consisting of natural flax fibers and natural cork core materials performed similarly to their counterparts made of synthetic glass fibers and synthetic honeycomb core materials in the investigation.

At the end of 20th and 21st centuries, the researcher and industrials have increased the use of natural fibers instead the synthetic ones because of the environmental and climatic issue, their lightness and goods mechanical properties compared to glass fibers in the fields of automobiles, locomotives, marine structures, and commercial applications [52,53]. Environmental protection challenges have recently received more attention globally. The fact that natural fibers are based on renewable plants and can be easily biodegraded has encouraged additional study into this sector to increase the use of eco-friendly products. Natural fiber composite materials are such an appropriate material that they can replace synthetic composite for many practical applications where we need high strength and low density. Pineapple leaf fiber (PALF) [54–56], palm, hemp [57,58], alfa, jute [42,52,59], cotton, bamboo, flax [60], silk [46,48], kenaf [43,49,61], and many others have been used in recent studies and the development of natural fiber composite structures. Table 1 compares natural and glass fibers and demonstrates in plain terms whether one has advantages over the other in several situations.

New bio-sandwich pipelines are a vital feature of today's and tomorrow's energy and industrial sectors, allowing for the transportation of different energy sources such as hydrogen as well as natural gas. Using natural fibers as the skin of the sandwich structures may provide a multifunctional, environmentally friendly structure. Several research efforts are being conducted to replace synthetic skins with composites made from natural fibers [51,60,65–67].

Table 1
Comparison of glass fiber and natural fibers.

Properties	Glass fiber	Natural fiber	Ref
Cost (US$/ton)	1200–1800	200–1000	[62]
Energy (GJ/ton)	30	4	
Density (g/cm^3)	2.4	1.2–1.6	[63]
Renewability	Non renewable	renewable	[64]
Recyclability	no	yes	
Energy consumption	High	Low	
Disposal	non-biodegradable	biodegradable	
Health risk when inhaled	Yes	No	
CO_2 emission	high	low	

Boria et al. [68] studied the response to low-velocity impact of sandwich structures with thin flax/epoxy face-sheets and an agglomerated cork core by using a non-linear dynamic FE model solved using LS-DYNA. Their findings demonstrated that agglomerated cork can be a renewable alternative to standard synthetic foam materials, as well as control damage extension and provide high energy absorption. An analytical model of a hybrid vessel with the goal of building an enhanced high hydrogen pressure storage vessel was created by Hocine et al. [69]. This analytical model provides a precise solution for stresses and strains on the hybrid model's cylinder section subjected to thermo-mechanical static loading and hydrogen leakage. For all this reasons, the present paper is focused to realize an analytical and numerical behavior study of bio composite sandwich pipe under internal pressure.

2. Problem description

The aim of this analysis is to evaluate the potential applications of eco-composites based on natural fibers such as jute and PALF bio-fibers in order to replace synthetic skins fibers of sandwich pipes in the natural gas pipeline industry. A failure analysis of biocomposite sandwich pipe under internal pressure, where the skins are based on bio-composite fibers is established. Analytical and 3D numerical models are developed which provides an exact solution for stresses, strains and displacement through the thickness of skins and core.

3. Presentation of analytical and FEM models

Considering a sandwich composite made up of three adjacent hollow cylinders that correspond to the two multilayered skins (upper and lower) and the epoxy core from inside to outside, of component of the transportation pipelines under internal pressure P (See Fig. 1), where the radius r is as follows: $r_i \le r \le r_o$.

3.1. Analytical model

For the analytical model, all displacements, strains, and stresses are independent of Θ for the axisymmetric sandwich pipe. The radial displacements r are independent of axial displacements. Z as well as axial coordinates is not dependent on the radial ones. Therefore, the displacements are:

$$U_r = U_r(r), U_\theta = U_\theta(r,z), U_z = U_z(Z) \tag{1}$$

The strain-displacement relations can be expressed as:

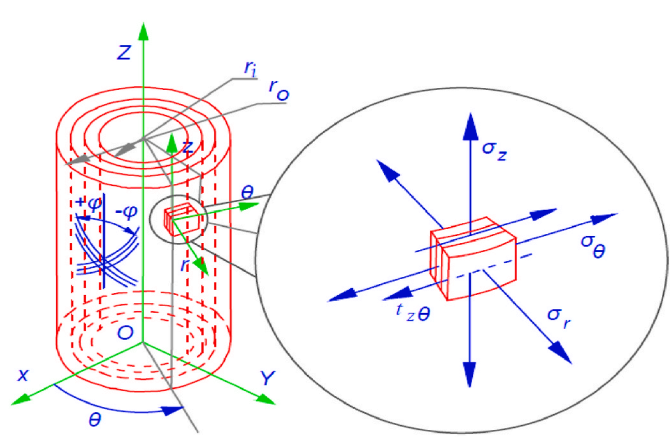

Fig. 1. Geometry of the sandwich pipe and wall stress components.

$$\begin{cases} \varepsilon_r^{(k)} = \dfrac{\mathrm{d}U_r^{(k)}}{\mathrm{d}_r}, \varepsilon_\theta^{(k)} = \dfrac{U_r^{(k)}}{r}, \varepsilon_z^{(k)} = \dfrac{\mathrm{d}U_z^{(k)}}{\mathrm{d}_z} = \varepsilon_0 \\ \gamma_{zr}^{(k)} = 0, \gamma_{\theta r}^{(k)} = \dfrac{\mathrm{d}U_\theta^{(k)}}{\mathrm{d}_r} - \dfrac{U_\theta^{(k)}}{r}, \gamma_{z\theta}^{(k)} = \dfrac{\mathrm{d}U_\theta^{(k)}}{\mathrm{d}_z} = \gamma_0 r \end{cases} \quad (2)$$

The general stress-strain relationship for each k-component exposed to axisymmetric thermo-mechanical loading [69] is shown below:

$$\begin{Bmatrix} \sigma_z \\ \sigma_\theta \\ \sigma_r \\ \tau_{\theta r} \\ \tau_{zr} \\ \tau_{z\theta} \end{Bmatrix} = \begin{bmatrix} C_{11} & C_{12} & C_{13} & 0 & 0 & C_{16} \\ C_{12} & C_{22} & C_{23} & 0 & 0 & C_{26} \\ C_{13} & C_{23} & C_{33} & 0 & 0 & C_{36} \\ 0 & 0 & 0 & C_{44} & C_{45} & 0 \\ 0 & 0 & 0 & C_{45} & C_{55} & 0 \\ C_{16} & C_{26} & C_{36} & 0 & 0 & C_{66} \end{bmatrix}^{(k)} \begin{Bmatrix} \varepsilon_z - \alpha_z \Delta T \\ \varepsilon_\theta - \alpha_\theta \Delta T \\ \varepsilon_r - \alpha_r \Delta T \\ \gamma_{\theta r} \\ \gamma_{zr} \\ \gamma_{z\theta} \end{Bmatrix}^{(k)} \quad (3)$$

The local balancing equations are as below in each k-component:

$$\frac{d\,\sigma_r^{(k)}}{dr} + \frac{\sigma_r^{(k)} - \sigma_\theta^{(k)}}{r} = 0 \quad (4)$$

The following differential equation is constructed by substituting the expression of radial and hoop stresses from equation (3) into equation (4) and applying equation (2):

$$\frac{d^2U_r^{(k)}}{dr^2} + \frac{1}{r}\frac{dU_r^{(k)}}{dr} - \frac{N_1^{(k)}}{r^2}U_r^{(k)} = \left[N_2^{(k)}\varepsilon_0 + N_3^{(k)}\Delta T\right]\frac{1}{r} + N_4^{(k)}\gamma_0 \quad (5)$$

Where:

$$N_1^{(k)} = \frac{C_{22}^{(k)}}{C_{33}^{(k)}};\ N_2^{(k)} = \frac{C_{12}^{(k)} - C_{13}^{(k)}}{C_{33}^{(k)}};\ N_3^{(k)} = \frac{K_3^{(k)} - K_2^{(k)}}{C_{33}^{(k)}};\ N_4^{(k)} = \frac{C_{26}^{(k)} - 2C_{36}^{(k)}}{C_{33}^{(k)}};\ \alpha_2^{(k)} = \frac{N_2^{(k)}}{1 - N_1^{(k)}};\ \alpha_3^{(k)} = \frac{N_3^{(k)}}{1 - N_1^{(k)}};\ \alpha_4^{(k)} = \frac{N_4^{(k)}}{4 - N_1^{(k)}} \quad (6)$$

And:

$$K_1^{(k)} = \alpha_z^{(k)}C_{11}^{(k)} + \alpha_\theta^{(k)}C_{12}^{(k)} + \alpha_r^{(k)}C_{13}^{(k)}\ \ K_2^{(k)} = \alpha_z^{(k)}C_{12}^{(k)} + \alpha_\theta^{(k)}C_{22}^{(k)} + \alpha_r^{(k)}C_{23}^{(k)}\ \ K_3^{(k)} = \alpha_z^{(k)}C_{13}^{(k)} + \alpha_\theta^{(k)}C_{23}^{(k)} + \alpha_r^{(k)}C_{33}^{(k)}\ K_4^{(k)} = \alpha_z^{(k)}C_{16}^{(k)} + \alpha_\theta^{(k)}C_{26}^{(k)} + \alpha_r^{(k)}C_{36}^{(k)} \quad (7)$$

The value of $\beta^{(k)} = \sqrt{N_1^{(k)}}$ determines the solution of equation (5), and can be expressed as:

$$\text{For } \beta^{(k)} = 1 : U_r^{(k)} = D^{(k)}r + \frac{E^{(k)}}{r + r\,ln(r)\left(N_2^{(k)}\ \varepsilon_0 + N_3^{(k)}\Delta T\right)} + \alpha_4^{(k)}\gamma_0 r^2 \quad (8)$$

$$\text{For } \beta^{(k)} = 2 : U_r^{(k)} = D^{(k)}r^{\beta^{(k)}} + E^{(k)}r^{-\beta^{(k)}} + \left(\alpha_2^{(k)}\varepsilon_0 + \alpha_3^{(k)}\Delta T\right)r + \frac{N_4^{(k)}}{2}\gamma_0 r^2\ \ln(r) \quad (9)$$

$$\text{For } \beta^{(k)} \neq 1\ or\ (2) : U_r^{(k)} = D^{(k)}r^{\beta^{(k)}} + E^{(k)}r^{-\beta^{(k)}} + (\alpha_2^{(k)}\varepsilon_0 + \alpha_3^{(k)}\Delta T + \alpha_4^{(k)}\gamma_0 r^2 \quad (10)$$

The superscript k is such as: $k \in [1, w]$ where:

$$w = n_s + n_c + n_s \quad (11)$$

The continuity conditions for the displacements and stresses in the interfaces lead to.

- The radial displacements' continuity is determined by:

$$\forall k\ [1, w-1], U^{(k)}\left(r_{ext}^{(k)}\right) = U^{(k+1)}\left(r_{ext}^{(k)}\right) \quad (12)$$

- The continuity of the radial stress gives:

$$\begin{cases} \forall k\ [1, w-1], \sigma_r^{(k)}\left(r_{ext}^{(k)}\right) = \sigma_{ext}^{(k+1)}\left(r_{ext}^{(k)}\right) \\ \sigma_r^{(1)}(r_i) = -p_0 \\ \sigma_r^{(w)}(r_o) = 0 \end{cases} \quad (13)$$

- The axial equilibrium of a cylinder with closed ends is satisfied by the following relation:

$$2\pi\sum_{k=1}^{w}\int_{r^{(k-1)}}^{r^{(k)}} \sigma_z^{(k)}(r)rdr = \pi r_i^2 p_0 \quad (14)$$

- Because the torque is zero, the expression takes the form:

$$2\pi\sum_{k=1}^{w}\int_{r^{(k-1)}}^{r^{(k)}} \tau_{z\theta}(r)r^2dr = 0 \quad (15)$$

The equations that follow make it possible to express the vectors' deformations and stresses in the reference fiber.

$$\begin{cases} \varepsilon' = T_\varepsilon\ \varepsilon \\ \sigma' = T_\sigma\ \sigma \end{cases} \quad (16)$$

Where:

$$T_\sigma = \begin{bmatrix} \cos^2\varphi & \sin^2\varphi & 0 & 0 & 0 & 2\sin\varphi\cos\varphi \\ \sin^2\varphi & \cos^2\varphi & 0 & 0 & 0 & -2\sin\varphi\cos\varphi \\ 0 & 0 & 1 & 0 & 0 & 0 \\ 0 & 0 & 0 & \cos\varphi & -\sin\varphi & 0 \\ 0 & 0 & 0 & \sin\varphi & \cos\varphi & 0 \\ -\sin\varphi\cos\varphi & \sin\varphi\cos\varphi & 0 & 0 & 0 & \cos^2\varphi - \sin^2\varphi \end{bmatrix} \quad (17)$$

And:

$$T_\varepsilon = \begin{bmatrix} \cos^2\varphi & \sin^2\varphi & 0 & 0 & 0 & \sin\varphi\cos\varphi \\ \sin^2\varphi & \cos^2\varphi & 0 & 0 & 0 & -\sin\varphi\cos\varphi \\ 0 & 0 & 1 & 0 & 0 & 0 \\ 0 & 0 & 0 & \cos\varphi & -\sin\varphi & 0 \\ 0 & 0 & 0 & \sin\varphi & \cos\varphi & 0 \\ -2\sin\varphi\cos\varphi & 2\sin\varphi\cos\varphi & 0 & 0 & 0 & \cos^2\varphi - \sin^2\varphi \end{bmatrix} \quad (18)$$

The Tsai-Wu criterion is introduced in the analytical model in order to evaluate the sandwich pipe strength:

$$F_{11}\left(\sigma_x^{(k)}\right)^2 + F_{22}\left(\sigma_y^{(k)}\right)^2 + F_{66}\left(\sigma_{yx}^{(k)}\right)^2 + 2F_{12}\sigma_y^{(k)}\sigma_x^{(k)} + F_1\sigma_x^{(k)} + F_2\sigma_y^{(k)} \leq 1 \quad (19)$$

With:

$$F_{11} = \frac{1}{\sigma_{xU}\ \sigma_{xU}'};\ F_{22} = \frac{1}{\sigma_{yU}\ \sigma_{yU}'};\ F_{12} = -\frac{1}{2}\frac{1}{\sqrt{\sigma_{yU}\ \sigma_{yU}'\ \sigma_{xU}\ \sigma_{xU}'}}\ F_{66} = \frac{1}{\sigma_{yxU}^2};\ F_1 = \frac{1}{\sigma_{xU}} - \frac{1}{\sigma_{xU}'};\ F_2 = \frac{1}{\sigma_{yU}} - \frac{1}{\sigma_{yU}'} \quad (20)$$

The solutions are obtained by using the MATLAB numerical code. The results are represented as functions of the non-dimensional ratio R:

$$R = \frac{r - r_i}{r_o - r_i} \quad (21)$$

3.2. FEM model

In order to validate our analytical approach, finite element simulations with ANSYS 18.1 and 3D elements are used in our study: Solid186 for the isotropic material (epoxy) and layered Solid186 for the orthotropic material (composites). A higher-order 3D element with quadratic displacement behavior is the ANSYS SOLID 186 element [70], which is shown in Fig. 2. The element contains 20 nodes, each with three degrees of freedom (translations in the three nodal directions). The element may be used as a structural solid or a layered solid element and is suitable for meshing irregular solids. The numerical model presents a uniform mesh of the global geometry, characterized by: 43,911 nodes and 8640 quadratic elements. Fig. 3 illustrates the entire FE model as well as its characteristics.

3.3. Geometry, materials and loading

The sandwich pipe configuration has an inner radius of 60 mm, a core-layer thickness of 10 mm, a skin-layer thickness of 0.27 mm and a length of 100 mm.

In the current study, two types of bio-skin material based on jute and pineapple leaf fibers compared to glass fibers were carried out. The skin materials characteristics are shown in Table 2. The core epoxy is shown in Table 3. The used layered skin stacking sequences are listed in Table 4.

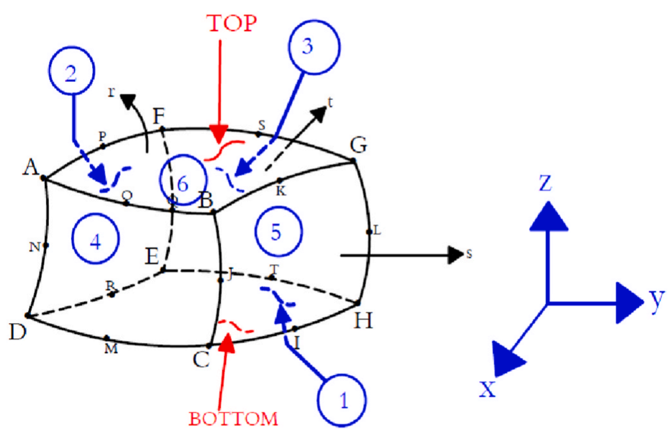

Fig. 2. The meshing element used for finite element models.

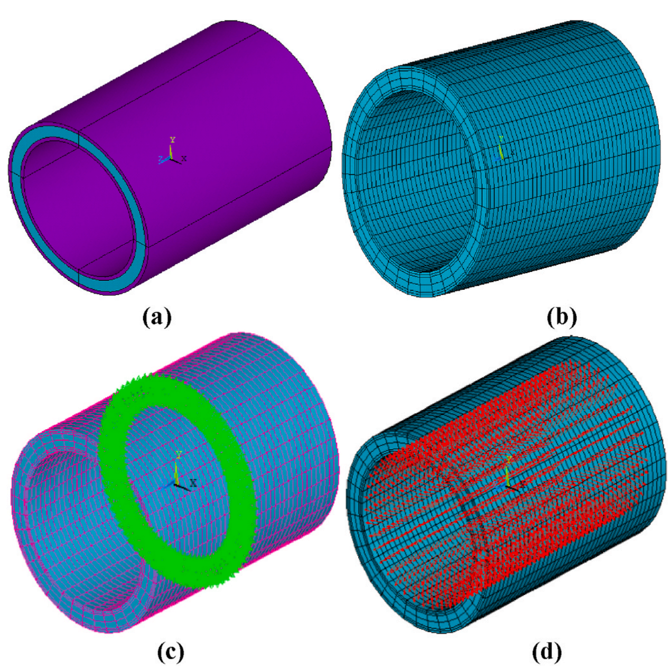

Fig. 3. The sandwich pipe structure. (a) The geometry, (b) the mesh, (c) boundary conditions, and (d) loading of the numerical model.

Table 2
Material properties of Jute/epoxy, PALF/epoxy and glass/Epoxy in the UD orthotropic frame.

Properties/Material	Jute/epoxy		Glass/epoxy	PALF/epoxy	
E_1 [GPa]	12.5	[59]	40	19.08	[50]
$E_2 = E_3$ [GPa]	5.633		10	7.86	
$G_{12} = G_{13}$ [GPa]	7.24		4.95	2.74	
G_{23} [GPa]	2.10		3.34	2.97	
$\nu_{12} = \nu_{13}$	0.3395		0.32	0.32	
ν_{23}	0.3395		0.495	0.32	
α_L [°C^{-1}]	40×10^{-6}		0.006×10^{-6}	40×10^{-6}	
Xt	55		2000	55	
Xc	55		750	55	
Yt	62		60	62	
Yc	62		160	62	
SI	27.5		200	27.5	

Table 3
Material properties of epoxy in the UD isotropic frame.

Material/ Properties	Young's modulus [GPa]	Poisson's Ratio	Shear modulus [GPa]	Ref
Epoxy **core**	4.1	0.41	1.453	[55]

Table 4
Stacking sequences of sandwich pipe parts with Epoxy core.

Stacking sequence of sandwich pipe parts	
Seq 1	[$[\pm 60]_2$/**core**/$[\pm 60]_2$]
Seq 2	[$[\pm 60]_6$/**core**/$[\pm 60]_6$]
Seq 3	[$[\pm 60]_9$/**core**/$[\pm 60]_9$]
Seq 4	[$[\pm 60]_{10}$/**core**/$[\pm 60]_{10}$]

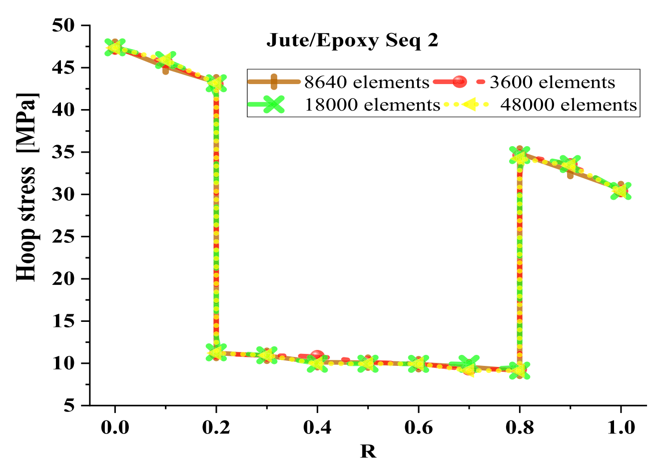

Fig. 4. Analysis of mesh convergence for finite elements of hoop stress distributions versus R.

The internal pressure applied to the sandwich pipe is 6 MPa. This pressure threshold was chosen in order to remain within the elastic range.

4. Analytical and FEM analysis

4.1. Analytical and numerical confrontation results

To validate the accuracy of our results, we performed a mesh convergence on the hoop stress of jute/epoxy along a non-dimensional radial distance. We've clearly arrived at a convergent solution.

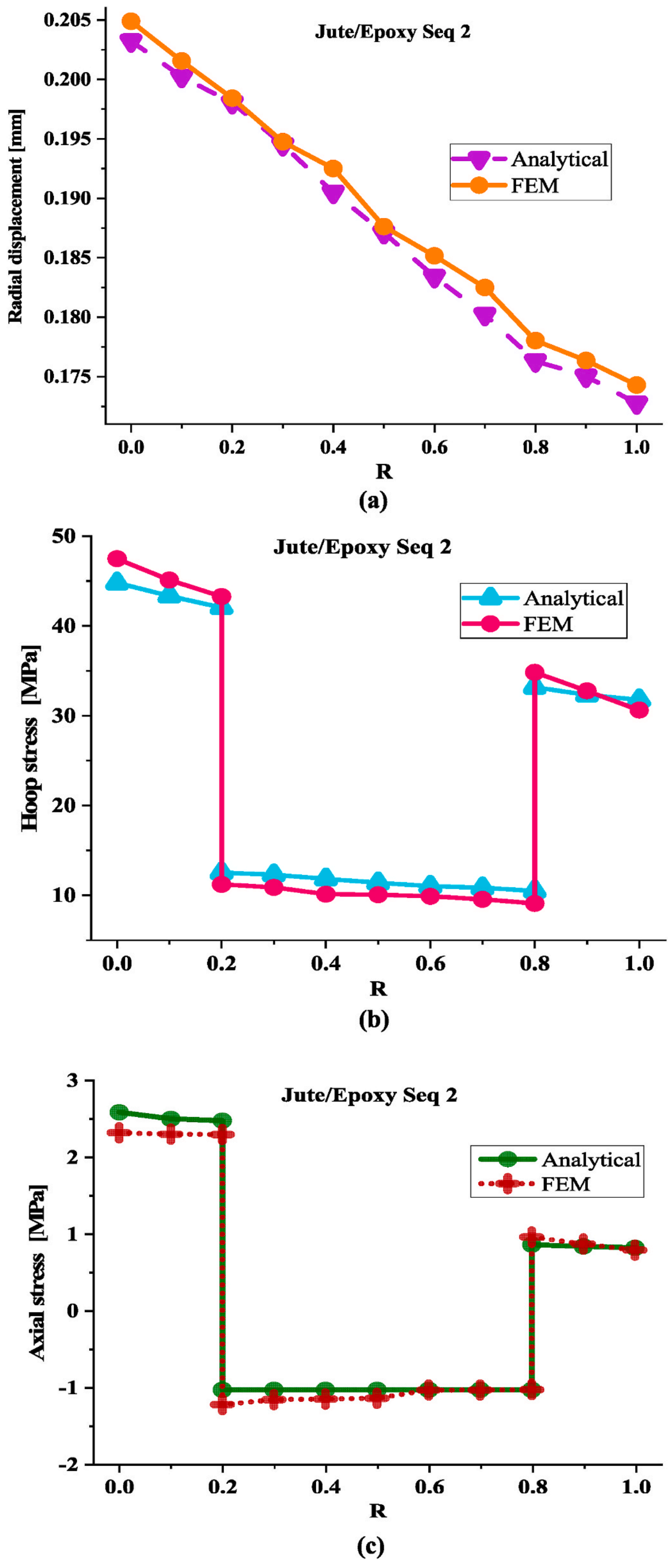

Fig. 5. Comparison of analytical and numerical results of Jute/epoxy. (a) Radial displacement, (b) Hoop stress and (c) Axial stress distributions versus R.

Fig. 4 summarizes the results of the convergence analyses based on adjusting the number of elements in the mesh.

Before developing the analytical results, a comparison is made between the analytical and FEM results.

Fig. 5 represents the comparison between both analytical (developed using Matlab) and numerical results obtained by means of commercial software (ANSYS 18.1) for the radial displacement, hoop and axial stress. This comparison shows a very good agreement and demonstrates that the responses of the structures are relatively well anticipated.

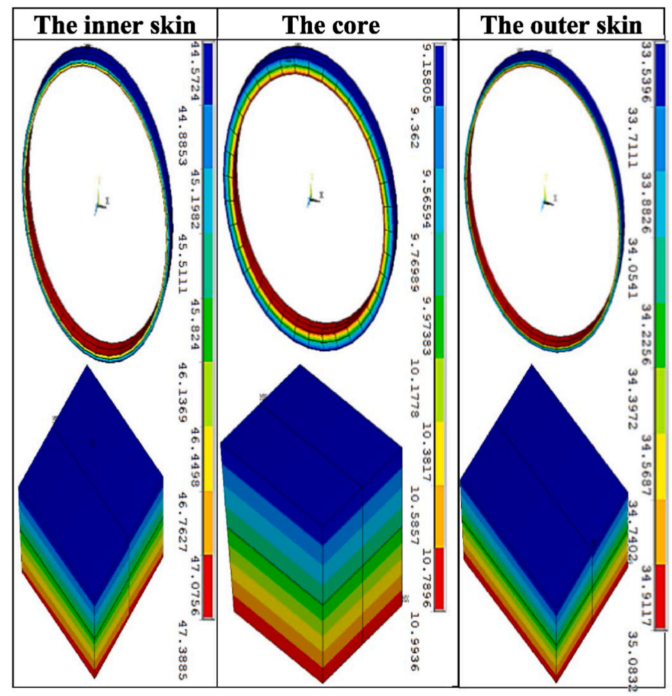

Fig. 6. The evolution of Hoop stress distribution for the sandwich pipe parts (inner, outer skins and the core) through thickness.

A comparison of stress, strain and radial displacement distributions through the wall thickness in the sandwich pipes is established, between synthetic and natural composite materials design as glass/epoxy, PALF/epoxy and jute/epoxy for the same stacking sequence as shown in Table 4.

The hoop stress distributions over the wall thickness of the sandwich pipe components (the inner and outer skins, as well as the core) using the color FE contour presented in Fig. 6.

The inner skin has the maximum stress distribution values compared to the outer skin and core.

4.2. *Analytical analysis results*

Fig. 7(a) shows the distribution of radial stress through the thickness of the sandwich pipe. For the three materials, a compressive radial stress increases from the inner skin to the outer through the core of the sandwich pipe. The maximum radial stress of −6 MPa is found at the inner skin which decries to zero at the outer skin, which reflects the boundary conditions applied.

The findings of the hoop and axial stress distributions between the core and the skins demonstrate a large variation for the multi-layered composite based on glass compared to natural fibers PALF and jute because these observations reveal the large anisotropic properties of glass.

The hoop stress presented in Fig. 7 (b) is a tensile state. The skin layers are subjected to significantly greater stresses which are about ten times compared to the core layer one. Moreover, the stress of inner skin is more than double compared to the outer skin. The jute/epoxy and PALF/epoxy sandwiches are less sensitive compared to glass/epoxy, where the stress magnitude is lower. The same remarks characterize the axial stress distribution, with a compression state being recorded in the core for all materials compared. The ratio between hoop stress and axial stress which is about ten reflects the internal pressure applied to the structure, and it can lead to a discontinuity between the core and the

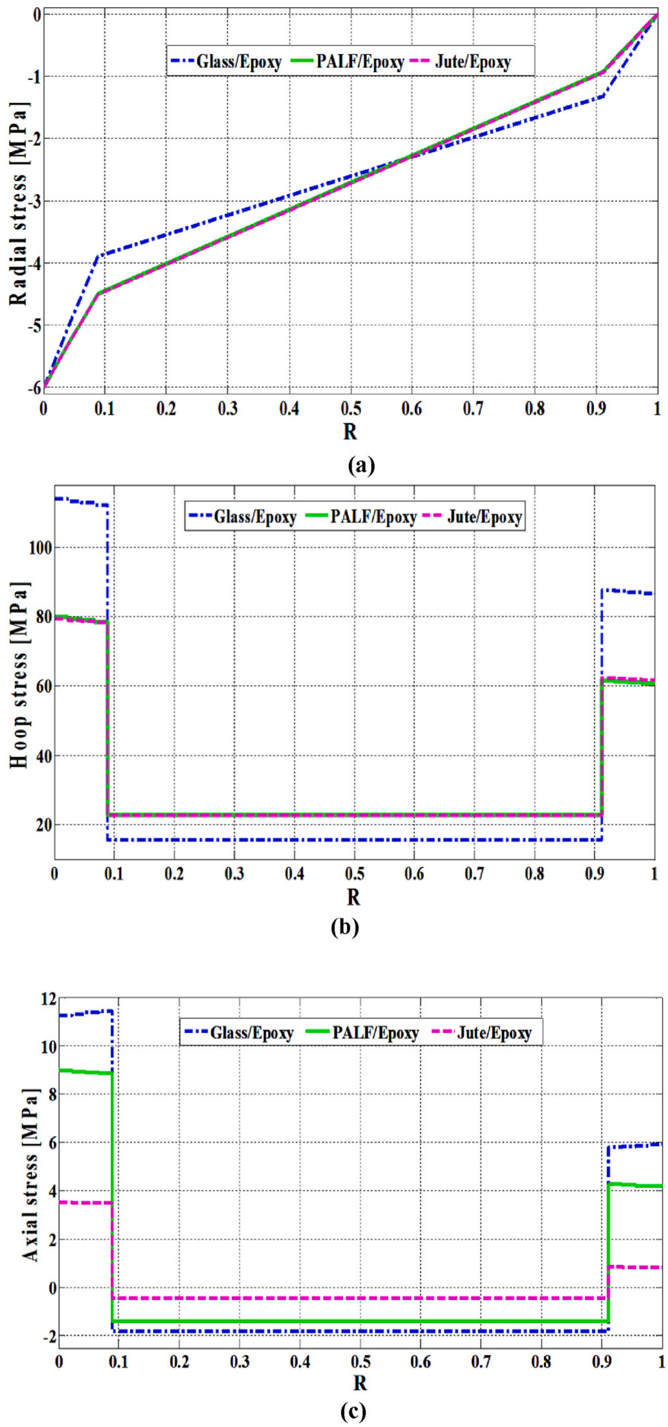

Fig. 7. The evolution of: (a) Radial stress, (b) Hoop stress and (c) Axial stress distributions versus R of Seq 1.

upper layer of the lower skin and the inner layer of the upper skin, (Fig. 7 (c)).

Fig. 8 shows the shear stresses distribution through the radius which is predominantly carried by the skins, with the sign of shear stress alternating through plies. The shear stress jump occurs depending on the layer fibers orientations between 60 and -60°, while, it is around zero in the core layer. The essential function of the sandwich core is to transmit, through shearing, the mechanical actions from one skin to the other. In terms of shear behavior, the stress magnitudes obtained for the bio-composite are better than those of the synthetic.

Fig. 9 shows a quasi-linear behavior of the variation of radial displacement through the radius. The structure's stiffness allows for a progressive decrease in radial displacement from one layer to another, which is determined by the material properties of the composite used as well as the stacking sequence of the lower and upper skins. The passage from one layer to another for skins or from skin to core translates the continuity of displacement imposed by the model. The magnitudes of radial displacement show that synthetic structures based on glass/epoxy undergo lower radial swelling compared to that of biocomposite.

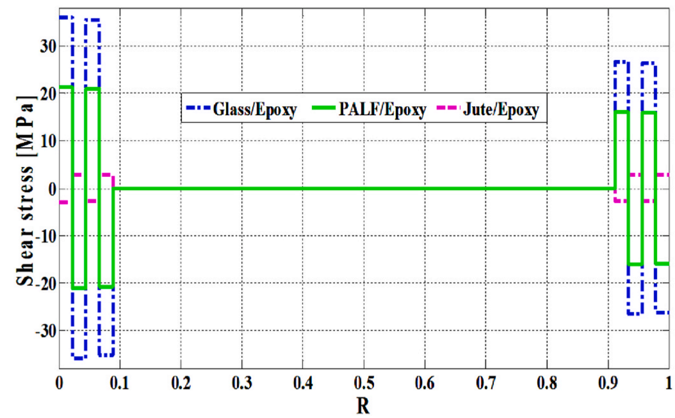

Fig. 8. The evolution of shear stress distributions of the three composites versus R of Seq 1.

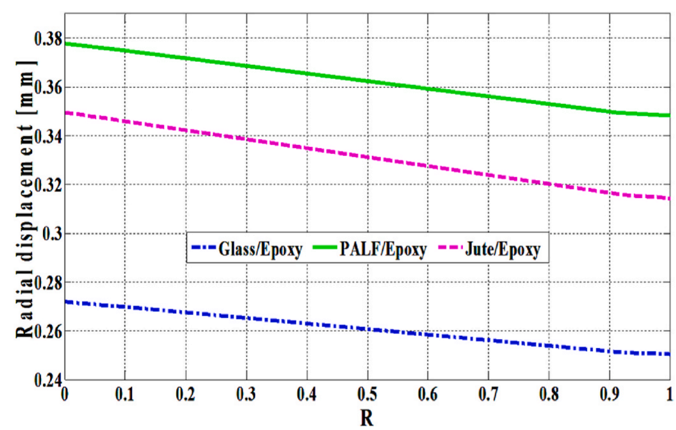

Fig. 9. The evolution of radial displacement distributions versus R of Seq 1.

The axial strain versus R is constant which reflect the impose boundary conditions and negligible compared to hoop strain due to loading mode (pure internal pressure). While, it depends on the material of the skin and the largest values is obtained for PALF/epoxy, followed by Glass/epoxy and the lowest is attributed to jute/epoxy (Fig. 10 (a)).

The hoop strain versus R is quasi-linear regressive and the maximal values are located at the internal wall of the pipes for the three materials investigated where the damage can be initiated (Fig. 10 (b)).

The pressure tested about 6 MPa represents a ratio of 2–3 of the service pressure, estimated 3 MPa which gives a very good safety margin for using biocomposites for manufacturing sandwich pipes.

Fig. 10 (c) shows the distribution of radial strain through the wall thickness, for the three different types of materials, where discontinuous variation is registered at the interface between the skin and the core and show compression state. The jute/epoxy has the largest radial strain in the internal part of the skin, followed by the PALF/epoxy, and the lowest for the glass/epoxy.

The TSAI-WU criterion allows us to determine the rupture limit of the most stressed internal layers according to the increment of the loading pressure for the material configurations chosen in this work. Sandwich

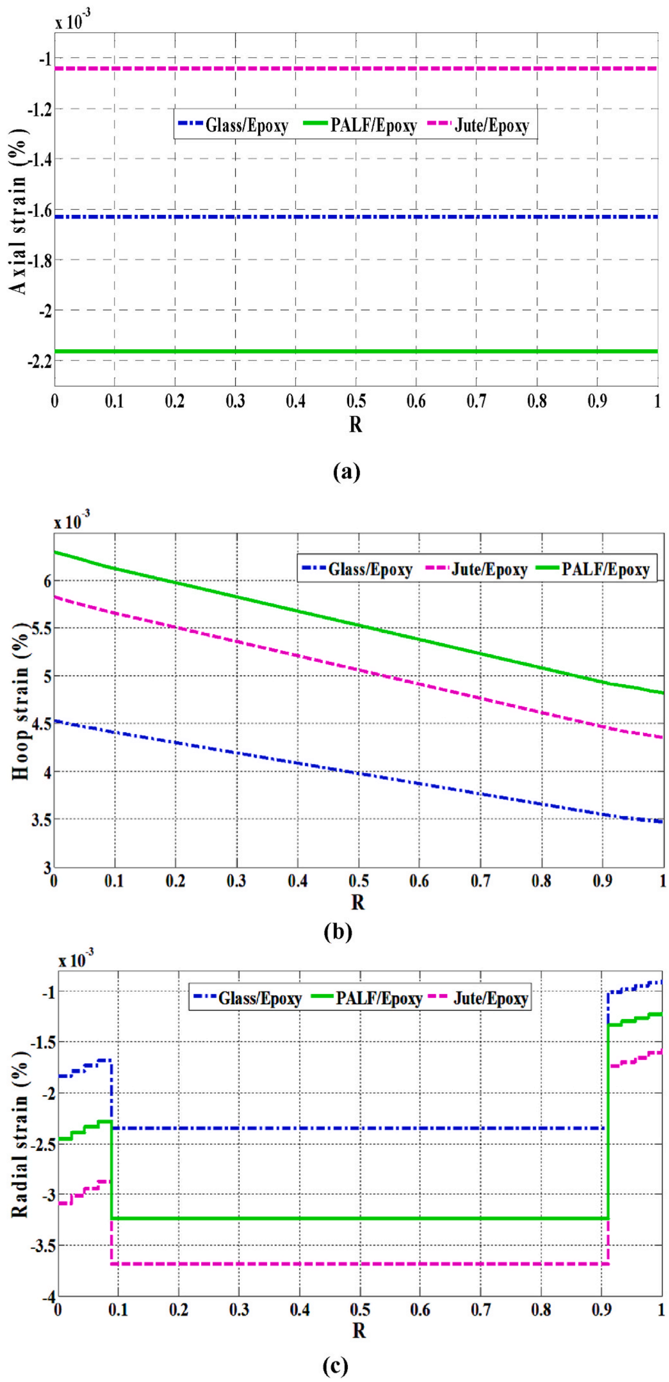

Fig. 10. The evolution of (a) Axial strain, (b) Hoop strain and (c) Radial strain distributions versus R of Seq 1.

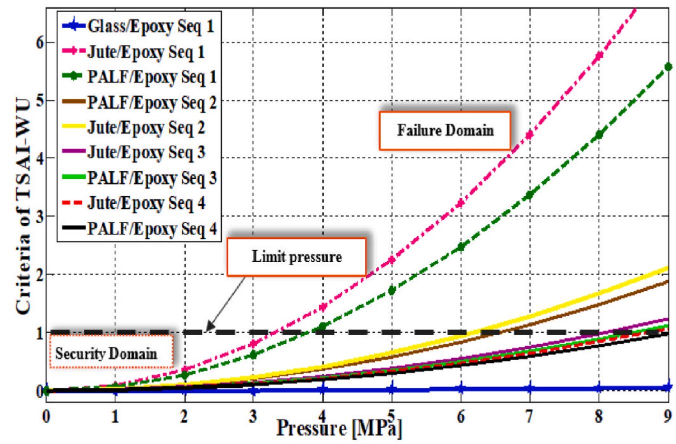

Fig. 11. Variations of TSAI-WU criterion versus internal pressure for various layer counts.

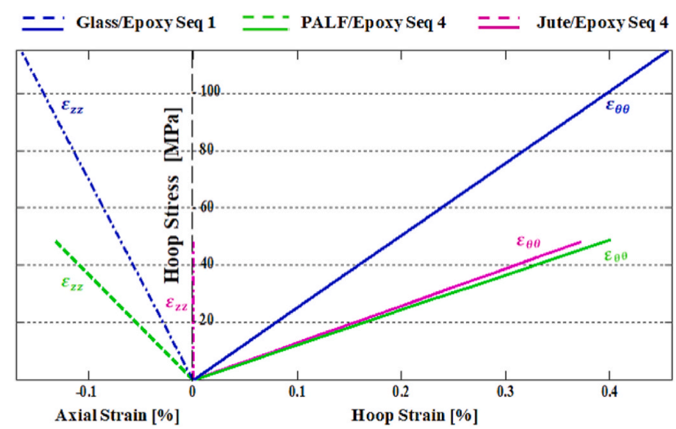

Fig. 12. The evolution of hoop stress versus hoop and axial strains.

pipes composed of glass/epoxy and two biocomposites, jute/epoxy and PALF/epoxy, are compared, (See Fig. 11).

It is noticed that gradually reinforcing biocomposite sandwiches by increasing the number of layers from Seq 1 to Seq 4 (see Table 4) increases their rigidity. The results show that for biocomposite sandwich pipe PALF/epoxy, the ultimate pressure is around 39 bars for Seq1, 65 bars for Seq2, 80 bars for Seq3, and finally 90 bars for Seq4. These results are better compared to sandwich pipes based on Jute/epoxy.

The limit pressure for a sandwich tube based on biocomposite reaches 85 bars for Seq4, allowing for a safety factor of 2.83 for PALF/epoxy and 2.66 for jute/epoxy. It is noticed that the overall process is operated at 30 bar of high pressure for hydrogen transportation pipelines [71].

The safety factors obtained for biocomposites are larger than 2.25 reported by Nghiep et al. for storage composite pressure vessels [72].

In other words, these results obtained allow us to have confidence in the substitution of synthetic fibers by natural ones while optimizing the number of layers.

Fig. 12 shows the analytic response of sandwich pipe under pure internal pressure which is in good agreement with the evolution of hoop stress versus axial and hoop strains.

The jute/epoxy has the best results (i.e., having the smallest values of hoop stress, axial and hoop strains) followed by the PALF/epoxy and the glass/epoxy.

5. Conclusion

This analysis, based on analytical and numerical methods is established to evaluate the potential applications of eco-composites sandwich pipes under pure internal pressure in order to replace synthetic composite (glass/epoxy). The findings lead to the following conclusions.

- The comparison of the analytical and FEM results of radial displacement, stress and strain reveals a good agreement.
- The hoop and axial stress show that the inner skins are significantly stressed compared to the outer. This can lead to the initiation of progressive damage at the inner wall of the sandwich tube which imposes to increase the number of layers of the internal skin compared to the external one.

- The results of shear stress confirm that the core part of the sandwich tube doesn't contribute to the resistance of shearing state which is supported just by the skin parts.
- In terms of hoop strain, the increase in the number of layers of natural fiber-based skins leads to a superior response of biosandwich compared to synthetic sandwich in terms of stiffness.
- The optimization of the number of natural fiber-based skins layers is essential to quality/price ratio.
- The results of axial strain show that the structure is compressed in the axial direction. Where the jute/epoxy demonstrates a good behavior compared to the glass/epoxy.
- The results of the hoop strain show a swelling of the sandwich tube, which is more noted for the natural fibers composite compared to the synthetic fiber.
- The radial strain results indicate a state of compression of the sandwich tube wall across the thickness, with a concentration at the core.
- The TSAI-WU criterion is used to prevent failure of the sandwich pipe in function of the increasing of internal pressure loading. The gradual reinforcing of bio-composite sandwiches by raising the number of layers elevates their rigidity.
- The pressure studied in this work is a factor of three of the service pressure, which is anticipated to be 30 bars. This affords a very good safety margin when using biocomposites for manufacturing sandwich tubes.
- Substituting synthetic fibers by bio-fibers yields a satisfactory result by increasing the number of layers and can play the same role at this stage of analysis.
- In order to have the optimum analytical and numerical tool design, the damage behavior that might occur in the skin and the core must be incorporated into the model. This behavior will be treated in the forthcoming study.

Funding

This work has been funded partially by the DGRSDT, Algeria and Portuguese national funds of FCT/MCTES (PIDDAC) through the base funding from the UIDB/00690/2020 (CIMO) research unit.

Credit author statement

Conceptualization: G.H and A.H; Data curation: G.H., A.H. and A.M.; Investigation: G.H; A.H, and A.M.; Methodology: G.H; A.H, A.M, A.B, and J.R; Resources: G.H, A.M, A.H, J.R, and M.H.D; Software: G.H, A.H, and A.M.; Supervision: A.H, A.B, J.R, M.H.D, and O.M; Validation: G.H, A.H, A.M, A.B, J.R, and M.H.D; Writing – original draft: G.H, A.H, A.M, A.B, J.R, M.H.D and O.M. Writing – review & editing: G.H, A.H, and A.B. All authors have read and agreed to the published version of the manuscript

Declaration of competing interest

The authors declare that they have no known competing financial interests or personal relationships that could have appeared to influence the work reported in this paper

Data availability

Data will be made available on request.

Nomenclature

Roman letters

$D^{(k)}, E^{(k)}$	The integration constants
$F_{11}, F_{12}, F_{22}, F_{66}$ F_1, F_2	The standard Tsai-Wu parameters
n_c	Number of core layers
n_s	Number of skin layers
r	Radial direction
$r_{ext}^{(k)}$	Outer radius of the layer k [mm]
r_i	Inner radius of skins [mm]
r_o	Outer radius of skins [mm]
T_ε	Constraint base change matrices
T_σ	Deformation basis change matrices
U_r	Radial displacements [mm]
U_z	Axial displacements [mm]
U_θ	Circumferential displacements [mm]
w	Number of composite layers
Z	Axial direction

Greek letters

α_r, α_z, α_θ	Thermal expansion coefficients [10-5 °C-1]
γ_{zr}	Shear strain vector in the plan z-r
$\gamma_{z\theta}$	Shear strain vector in the plan z-Θ
$\gamma_{\theta r}$	Shear strain vector in the plan Θ-r
γ_0 and ε_0	The integration constants
ΔT	Temperature deviation [°C]
ε_r	Radial strain vector
ε_z	Axial strain vector
ε_θ	Circumferential strain vector
ε'	Deformation vector in the coordinate system
Θ	Circumferential direction
σ_{xu}	The tensile strengths of the composite material [MPa]
σ_{yu}	The Compressive strengths of the composite material [MPa]
σ_{yxu}	In the layer plane shear strength [MPa]

σ'	Stress vector in the coordinate system [MPa]
σ'_{xu}	In the direction of the fibers [MPa]
σ'_{yu}	In the transverse direction [MPa]
τ_{zr}	Shear strain vector in the plan $z-r$ [MPa]
$\tau_{z\theta}$	Shear strain vector in the plan $z-\Theta$ [MPa]
$\tau_{\theta r}$	Shear strain vector in the plan $\Theta-r$ [MPa]
φ	The winding angle (°)

References

[1] K. Arjomandi, F. Taheri, A New Look at the External Pressure Capacity of Sandwich Pipes, vol. 24, 2011, pp. 23–42, https://doi.org/10.1016/j.marstruc.2010.12.001.
[2] P. Laney, Use of Composite Pipe Materials in the Transportation of Natural Gas, July, 2002.
[3] A. Czapla, M. Ganesapillai, J. Drewnowski, Composite as a material of the future in the era of green deal implementation strategies, Processes 9 (2238) (2021) 1–20, https://doi.org/10.3390/pr9122238.
[4] C.V. Amaechi, A. Reda, I.A. Ja'e, C. Wang, C. An, Guidelines on composite flexible risers : monitoring techniques and design approaches, Energies 15 (2022), https://doi.org/10.3390/en15144982, 4982.
[5] Y. . Ma, Q., G. Tian, B. Zeng, R. Li, H. Song, Z. Wang, Gao, K. Zeng, Pipeline In-Line Inspection Method, Instrumentation and Data Management, 2021, https://doi.org/10.3390/s21113862 sensors.
[6] H.R. Vanaei, A. Eslami, A. Egbewande, A review on pipeline corrosion, in-line inspection (ILI), and corrosion growth rate models, *Int. J. Press. Vessel. Pip.*, no. Ili (2016), https://doi.org/10.1016/j.ijpvp.2016.11.007.
[7] A.H. Alamri, Localized corrosion and mitigation approach of steel materials used in oil and gas pipelines -an overview, Eng. Fail. Anal. (2020), 104735, https://doi.org/10.1016/j.engfailanal.2020.104735, 2020.
[8] G. Bolzon, G. Gabetta, Degradation Assessment and Failure Prevention of Pipeline Systems, 2021.
[9] Azam Ali, et al., Hydrophobic treatment of natural fibers and their composites—a review, J. Ind. Textil. 47 (8) (2018) 2153–2183, https://doi.org/10.1177/1528083716654468.
[10] M. Sun, H. Zhao, X. Li, J. Liu, Z. Xu, New evaluation method of failure pressure of steel pipeline with irregular-shaped defect, Appl. Ocean Res. 110 (2021), 102601, https://doi.org/10.1016/j.apor.2021.102601. March.
[11] M. Witek, Structural Integrity of Steel Pipeline with Clusters of 14 (852) (2021), https://doi.org/10.3390/ma14040852.
[12] K. Digheche, Z. Boumerzoug, M. Diafi, K. Saadi, INFLUENCE OF HEAT TREATMENTS ON THE MICROSTRUCTURE OF WELDED 23 (1) (2017) 72–78, https://doi.org/10.12776/ams.v23i1.879.
[13] C.K. Mukhopadhyay, R. Mulaveesala, Advances in Non-destructive Evaluation, he registered company Springer Nature Singapore Pte Ltd., 2019.
[14] T. Zheng, Z. Liang, L. Zhang, S. Tang, Z. Cui, Safety assessment of buried natural gas pipelines with corrosion defects under the ground settlement, Eng. Fail. Anal. 129 (August) (2021), 105663, https://doi.org/10.1016/j.engfailanal.2021.105663.
[15] Y. Lee, G. Kim, K. Kim, S. Ko, W. Kim, J. Kim, Localized corrosion occurrence in low-carbon steel pipe caused by microstructural inhomogeneity, Mater. Artic. (2022), https://doi.org/10.3390/ma15051870.
[16] J. Narayan, E. Yanez, A. Angshu, P. Egberts, Tribology International Tribo-corrosion inhibition of AISI 4715 steel pipe carrying hydraulic fracturing fluid, Tribol. Int. 161 (2021), 107066, https://doi.org/10.1016/j.triboint.2021.107066. March.
[17] D. Zhou, et al., in: The Experiment Study to Assess the Impact of Hydrogen Blended Natural Gas on the Tensile Properties and Damage Mechanism of X80 Pipeline Steel, 2021, p. 2020, https://doi.org/10.1016/j.ijhydene.2020.11.267.
[18] E.S. Ameh, S.C. Ikpeseni, L.S. Lawal, A Review of Field Corrosion Control and Monitoring Techniques of the Upstream Oil and Gas Pipelines, 2015, pp. 67–73, https://doi.org/10.4314/njtd.v14i2.5.
[19] A. Royani, S. Prifiharni, G. Priyotomo, Corrosion Behavior of Low Carbon Steel Pipe in Condensate Environment 19 (3) (2022) 1–11, https://doi.org/10.48048/tis.2022.2072.
[20] X. Guo, L. Zhang, W. Liang, S. Haugen, Risk identification of third-party damage on oil and gas pipelines through the Bayesian network, J. Loss Prev. Process. Ind. (2018), https://doi.org/10.1016/j.jlp.2018.03.012.
[21] I. Quej-Ake, L.M., J.N. Rivera-Olvera, Y.d.R. Domínguez-Aguilar, I.A. Avelino-Jiménez, V. Garibay-Febles, Zapata-Peñasco, Analysis of the Physicochemical, Mechanical, and Electrochemical Parameters and Their Impact on the Internal and External SCC of Carbon Steel Pipelines, MDPi Mater., 2020, pp. 1–35, https://doi.org/10.3390/ma13245771.
[22] O. Bouledroua, Z. Hafsi, M.B. Djukic, S. Elaoud, The synergistic effects of hydrogen embrittlement and transient gas flow conditions on integrity assessment of a precracked steel pipeline, Int. J. Hydrogen Energy xxxx (2020), https://doi.org/10.1016/j.ijhydene.2020.04.262.
[23] I. Lapiga, A. Shchipachev, D. Osadchiy, Using of Artificial Neural Networks to Assess the Residual Resource of Trunk Pipelines, vols. 3–6, 2021, 02006, https://doi.org/10.1051/e3sconf/202122502006.
[24] H. Nykyforchyn, L. Unigovskyi, O. Zvirko, O. Tsyrulnyk, H. Krechkovska, Pipeline durability and integrity issues at hydrogen transport via natural gas distribution network, Procedia Struct. Integr. 33 (2019) 646–651, https://doi.org/10.1016/j.prostr.2021.10.071, 2021.
[25] V. Zapukhlyak, Y. Melnychenko, I. Okipnyi, L. Poberezhny, Y. Grudz, I. Okipnyi, Reliability assurance of gas-hydrogen mixture transportation by gas pipeline system, Procedia Struct. Integr. 36 (2021) 378–385, https://doi.org/10.1016/j.prostr.2022.01.049, 2022.
[26] M.M. Prabhakar, et al., An overview of burst , buckling , durability and corrosion analysis of lightweight FRP composite pipes and their applicability, Compos. Struct. 230 (September) (2019), 111419, https://doi.org/10.1016/j.compstruct.2019.111419.
[27] A. Maizia, A. Hocine, H. Dehmous, D. Chapelle, Prediction of reliability analysis of composite tubular structure under hygro-thermo-mechanical loading, Mech. Adv. Mater. Struct. 26 (4) (2019) 372–379, https://doi.org/10.1080/15376494.2017.1387329.
[28] I.Y. Sulu, S. Temiz, Failure and stress analysis of internal pressurized composite pipes joined with sleeves, J. Adhes. Sci. Technol. 4243 (October) (2017) 1–17, https://doi.org/10.1080/01694243.2017.1385376.
[29] A. Zubail, A. Traidia, M. Masulli, K. Vatopoulos, T. Villette, I. Taie, Carbon and energy footprint of nonmetallic composite pipes in onshore oil and gas flowlines, J. Clean. Prod. 305 (2021), 127150, https://doi.org/10.1016/j.jclepro.2021.127150.
[30] D. Chapelle, A. Hocine, S. Carbillet, M.L. Boubakar, Analysis of intermetallic swelling on the behavior of a hybrid solution for compressed hydrogen storage - Part II: finite element method simulation, Mater. Des. 36 (2012) 459–469, https://doi.org/10.1016/j.matdes.2011.11.056.
[31] M. Xia, H. Takayanagi, K. Kemmochi, Analysis of Multi-Layered Filament-Wound Composite Pipes under Internal Pressure, vol. 53, 2001.
[32] T. Wang, O. Menshykov, M. Menshykova, Modelling and Optimal Design of Thick-Walled Composite Pipes under in- Service Conditions, 2020, https://doi.org/10.1088/1757-899X/936/1/012046. October.
[33] S. Jansma, K. Technology, P. Cloos, E. Van Der Stok, K. Technology, TESTING SPOOLABLE REINFORCED FLEXIBLE PIPES AND LINER MATERIAL FOR HIGH-PRESSURE HYDROGEN TRANSPORT, 2020, pp. 1–10, 2020.
[34] H. Wang, M. Duan, C. An, J. Su, Lumped parameter thermal analysis of multilayered composite pipe with MicroPCM particles, Compos. Struct. 260 (2021), 113495, https://doi.org/10.1016/j.compstruct.2020.113495. August 2020.
[35] I.A. Guz, M. Menshykova, J.K. Paik, Thick-walled Composite Tubes for Offshore Applications : an Example of Stress and Failure Analysis for Filament-Wound Multi-Layered Pipes, vol. 5302, October, 2015, https://doi.org/10.1080/17445302.2015.1067019.
[36] A. Maizia, A. Hocine, H. Dehmous, Development of a reliability-mechanical : numerical model of mechanical behavior of a multilayer composite plate, Appl. Mech. Behav. Mater. Eng. Syst. (2017) 387–397, https://doi.org/10.1007/978-3-319-41468-3.
[37] J.C. Hastie, M. Kashtalyan, I.A. Guz, Analysis of filament-wound sandwich pipe under combined internal pressure and thermal load considering restrained and closed ends, Int. J. Pres. Ves. Pip. 191 (2021), 104350, https://doi.org/10.1016/j.ijpvp.2021.104350. November 2020.
[38] J. Yu, W. Xu, N. Chen, S. Jiang, S. Xu, Effect of dent defects on the collapse pressure of sandwich pipes, Thin-Walled Struct. 170 (2022), 108608, https://doi.org/10.1016/j.tws.2021.108608, 2022.
[39] J. Yang, et al., Collapse pressure of sandwich pipes with strain-hardening cementitious composite - Part 1 : experiments and parametric study, Thin-Walled Struct. 148 (2020), 106605, https://doi.org/10.1016/j.tws.2020.106605. September 2019.
[40] D. Fern, A. O. V, FEM-Based Evaluation of Friction and Initial Imperfections Effects on Sandwich Pipes Local Buckling, vol. 72, 2020, p. 102769, https://doi.org/10.1016/j.marstruc.2020.102769.
[41] M. Xia, K. Kemmochi, H. Takayanagi, Analysis of filament-wound sandwich pipe under internal pressure 9 (3) (2000) 223–239.
[42] D.E. Kari, A. Benmounah, A. Bezazi, B. Bezzazi, B. Baali, in: Evaluation of Circumferential Properties of Jute/Epoxy Tubes Manufactured by Filament Winding Based on the Fiber Orientation, 2021, pp. 459–468.
[43] S. Misri, M.R. Ishak, S.M. Sapuan, Z. Leman, The effect of winding angles on crushing behavior of filament wound hollow kenaf yarn fibre reinforced unsaturated polyester composites, Fibers Polym. 16 (10) (2015) 2266–2275, https://doi.org/10.1007/s12221-015-5447-y, 2015.
[44] F. Wang, L. Han, Analytical behavior of carbon steel-concrete-stainless steel double- skin tube (DST) used in submarine pipeline structure, Mar. Struct. 63 (2019) 99–116, https://doi.org/10.1016/j.marstruc.2018.09.001. April 2018.

[45] J. Zhang, Y. Ye, Y. Zhu, H. Yuan, Q. Qin, T. Wang, On axial splitting and curling behaviour of circular sandwich metal tubes with metal foam core, Int. J. Solid Struct. 202 (2020) 111–125, https://doi.org/10.1016/j.ijsolstr.2020.06.021.

[46] S. Ataollahi, S.T. Taher, R.A. Eshkoor, A.K. Ariffin, C.H. Azhari, Energy absorption and failure response of silk/epoxy composite square tubes, Experientia (Basel) 43 (2012) 542–548, https://doi.org/10.1016/j.compositesb.2011.08.019.

[47] Y. Wang, Z. Zhang, X. Xue, J. Zhou, Z. Song, Axial and lateral crushing performance of plate-lattice fi lled square sandwich tubes, Compos. Struct. 274 (2021), 114404, https://doi.org/10.1016/j.compstruct.2021.114404. July.

[48] R.A. Eshkoor, et al., in: Failure Mechanism of Woven Natural Silk/Epoxy Rectangular Composite Tubes under Axial Quasi-Static Crushing Test Using Trigger Mechanism, 2014, pp. 53–61, https://doi.org/10.1016/j.ijimpeng.2013.09.004.

[49] M.F.M. Alkbir, S.M. Sapuan, A.A. Nuraini, M.R. Ishak, Effect of geometry on crashworthiness parameters of natural kenaf fibre reinforced composite hexagonal tubes, J. Mater. 60 (2014) 85–93, https://doi.org/10.1016/j.matdes.2014.02.031.

[50] G. Habbar, A. Maizia, A. Hocine, M.H. Dhaou, R. João, Micromechanical analysis of a bio-sandwich application for cylinder under pressure, Compost Sci. 6 (69) (2022), https://doi.org/10.3390/jcs6030069.

[51] P. Sadeghian, D. Hristozov, L. Wroblewski, Experimental and analytical behavior of sandwich composite beams: comparison of natural and synthetic materials, J. Sandw. Struct. Mater. 20 (3) (2018) 287–307, https://doi.org/10.1177/1099636216649891.

[52] R. Sangamesh, N. Kumar, K.S. Ravishankar, S.M. Kulkarni, Mechanical characterization and finite element analysis of jute-epoxy composite, MATEC Web Conf 2014 (2018) 1–6, https://doi.org/10.1051/matecconf/201814402014.

[53] A. Merzoug, B. Bouhamida, Z. Sereir, Quasi-static and dynamic mechanical thermal performance of date palm/glass fiber hybrid composites, Ind. Textil. (2020) 1–23, https://doi.org/10.1177/1528083720958036.

[54] M. Asim, et al., A review on pineapple leaves fibre and its composites, Int. J. Polym. Sci. 2015 (2015), https://doi.org/10.1155/2015/950567.

[55] R. Potluri, V. Diwakar, K. Venkatesh, B. Srinivasa Reddy, Analytical model application for prediction of mechanical properties of natural fiber reinforced composites, Mater. Today Proc. 5 (2018) 5809–5818, https://doi.org/10.1016/j.matpr.2017.12.178.

[56] J. Naim, Study on mechanical properties of pineapple-glass fiber based polymer, Int. J. Mech. Eng. Autom. 4 (2017). January.

[57] R. Dragonetti, M. Napolitano, L. Boccarusso, M. Durante, A study on the sound transmission loss of a new lightweight hemp/bio-epoxy sandwich structure, Appl. Acoust. 167 (2020), 107379, https://doi.org/10.1016/j.apacoust.2020.107379.

[58] N. Elzayady, E. Elghandour, Fracture resistance of composite structurs from hemp bio-fibers, J. Adv. Eng. Trends 40 (2) (2021) 137–147, https://doi.org/10.21608/jaet.2020.44308.1059.

[59] S. Rajole, K.S. Ravishankar, S.M. Kulkarni, Performance study of jute-epoxy composites/sandwiches under normal ballistic impact, Def. Technol. 16 (4) (2020) 947–955, https://doi.org/10.1016/j.dt.2019.11.011.

[60] L. CoDyre, A. Fam, Axial strength of sandwich panels of different lengths with natural flax-fiber composite skins and different foam-core densities, J. Compos. Construct. 21 (5) (2017), 04017042, https://doi.org/10.1061/(asce)cc.1943-5614.0000820.

[61] N. Sapiai, A. Jumahat, J. Mahmud, Mechanical properties of functionalised CNT filled kenaf reinforced epoxy composites, Mater. Res. Express 5 (4) (2018), https://doi.org/10.1088/2053-1591/aabb63.

[62] H. Carvalho, H. Salman, M. Leite, Natural Fibre Composites and Their Applications : A Review, 2018, pp. 1–20, https://doi.org/10.3390/jcs2040066.

[63] Y. Gowda, T. Girijappa, S.M. Rangappa, Natural fibers as sustainable and renewable resource for development of eco-friendly composites, A Comprehensive Review 6 (September) (2019) 1–14, https://doi.org/10.3389/fmats.2019.00226.

[64] P. Wambua, J. Ivens, I. Verpoest, Natural fibres : can they replace glass in fibre reinforced plastics, Compos. Sci. Technol. 63 (2003) 1259–1264, https://doi.org/10.1016/S0266-3538(03)00096-4.

[65] M. Zwawi, A Review on Natural Fiber Bio-Composites, Surface Modifications and Applications, 2021.

[66] A. Ticoalu, T. Aravinthan, F. Cardona, A Review of Current Development in Natural Fiber Composites for Structural and Infrastructure Applications, 2010, pp. 1–5.

[67] M. Alhijazi, Q. Zeeshan, Z. Qin, B. Safaei, M. Asmael, Finite element analysis of natural fibers composites: a review, Nanotechnol. Rev. 9 (1) (2020) 853–875, https://doi.org/10.1515/ntrev-2020-0069.

[68] S. Boria, E. Raponi, F. Sarasini, J. Tirillò, L. Lampani, Green sandwich structures under impact: experimental vs numerical analysis, Procedia Struct. Integr. 12 (2018) 317–329, https://doi.org/10.1016/j.prostr.2018.11.084.

[69] A. Hocine, D. Chapelle, L.M. Boubakar, A. Benamar, A. Bezazi, Analysis of intermetallic swelling on the behavior of a hybrid solution for compressed hydrogen storage – Part I : analytical modeling, Mater. Des. 31 (2010) 2435–2443, https://doi.org/10.1016/j.matdes.2009.11.048.

[70] E.J. Barbero, Finite Element Analysis of Composite Materials Using Ansys®, second ed., no. January 2008, CRC Press, Boca Raton, 2013.

[71] S. Timmerberg, M. Kaltschmitt, Hydrogen from renewables : supply from North Africa to central Europe as blend in existing pipelines – potentials and costs, Appl. Energy 237 (2020) 795–809, https://doi.org/10.1016/j.apenergy.2019.01.030. November 2018.

[72] B. Nghiep, H. Seok Roh, D.R. Merkel, K.L. Simmons, A predictive modeling tool for damage analysis and design of hydrogen storage composite pressure vessels, Int. J. Hydrogen Energy 46 (39) (2021) 20573–20585, https://doi.org/10.1016/j.ijhydene.2021.03.139.